The Vibration Response of a Cantilevered Rectangular Cylinder in Cross-Flow Oscillation

Mizuyasu Koide
Life Engineering Research Center, Niigata Sangyo University, 4730 Karuigawa, Kashiwazaki, Niigata, 945-1393, Japan
e-mail: mkoide@life-eng.nsu.ac.jp

Yuuki Kubo
Toray Engineering Co., Ltd., Seta3-3-25, Ootsu, Shiga, 520-2134, Japan
e-mail: yuki_kubo@toray-eng.co.jp

Tsutomu Takahashi
Department of Mechanical Engineering, Nagaoka University of Technology, 1603-1 Kamitomioka, Nagaoka, Niigata, 940-2188, Japan
e-mail: ttaka@mech.nagaokaut.ac.jp

László Baranyi
Department of Fluid and Heat Engineering, University of Miskolc, H-3515, Miskolc-Egyetemváros, Hungary
e-mail: arambl@uni-miskolc.hu

Masataka Shirakashi
Department of Mechanical Engineering, Nagaoka University of Technology, 1603-1 Kamitomioka, Nagaoka, Niigata, 940-2188, Japan
e-mail: kashi@mech.nagaokaut.ac.jp

[DOI: 10.1115/1.1792255]

Introduction

It is well known that a large-amplitude oscillation called galloping [1–3] is generated, in addition to Kármán vortex excitation, for rectangular cylinders supported perpendicularly to a uniform flow when the slenderness b/d is in the range of 0.6 to 2.8 (d=height, b=streamwise length of the rectangular cross-section). The basic aerodynamic excitation mechanism of the cross-flow galloping of a rectangular cylinder is explained by the quasi-steady nonlinear aerodynamic theory developed by Parkinson et al. [4]. In this theory, the relative attack angle plays an important role in the excitation mechanism of galloping. Also, as was shown by Deniz and Staubli [5], the attack angle of a fixed rectangular cylinder strongly affects the vortex shedding frequency and lift.

Although the mechanism of pure cross-flow oscillation for a circular and rectangular cylinder is becoming clear, as seen in the recent paper [6], a slight difference in support conditions may affect strongly the oscillation behavior. The specific aim of this paper is to present the effect of attack angle fluctuation on the cross-flow oscillation behavior of a rectangular cylinder supported by a cantilever plate-spring system.

Contributed by the Fluids Engineering Division for publication in the JOURNAL OF FLUIDS ENGINEERING. Manuscript received by the Fluids Engineering Division August 6, 2003; revised manuscript received March 15, 2004. Associate Editor: H. Johari.

Experimental Apparatus and Measurements

Three rectangular cylinders with an equal height, $d=26$ mm, and a slenderness of $b/d=0.5$, 1.0, and 2.0 were used. These were chosen since $b/d=0.5$ is less than the galloping range and $b/d=2.0$ is higher than the Kármán vortex excitation range. Hereafter, the rectangular cylinders with $b/d=0.5$, 1.0, and 2.0 are expressed as Cylinder I, Cylinder II, and Cylinder III, respectively.

Experiments were carried out in a blow-down type wind tunnel with a measuring section of 320(H)×320(W)×1000(L) mm as shown in Fig. 1. The turbulence level in the measuring section was less than 0.6%. The cylinder was placed in the wind tunnel horizontally, perpendicular to the free stream. The blockage ratio was 8%. The cylinder was supported at both ends outside the measuring section. End plates were attached to the cylinder to remove influence of flow through slots on the sidewalls of the measuring section [7].

In order to investigate the influence of attack angle fluctuation superimposed on cross-flow oscillation, i.e., Kármán vortex excitation and galloping, the cylinder was supported by cantilever plate springs in three ways as shown in Fig. 2. When the cylinder is supported by the twin plate spring as in Fig. 2*a*, its motion is almost purely translational in the z direction. When the cylinder is supported by the single plate spring, a geometrical attack angle α_g is superposed due to angular deflection at the end of a cantilever beam. Thus α_g fluctuation is generated synchronizing with cylinder displacement Z. The phase difference ϕ between α_g and Z is zero (i.e., "in-phase") when the cylinder is supported against the flow as in Fig. 2*b*, and $\phi=\pi$ ("anti-phase") when the cylinder is supported following the flow as in Fig. 2*c*. The magnitude of geometrical attack angle α_g is given by $|\alpha_g|=3|Z|/(2l)$, where l is the cantilever beam length. The absolute value of α_g reaches 6° at $Z=5$ mm, the maximum displacement in this experiment. The natural frequency f_n, the effective mass m_e, and the logarithmic damping factor δ were determined through a free damping oscillation experiment in otherwise quiescent air. These parameters, as well as the cantilever length l and the spring constant k, were virtually equal for all the cylinders and irrespective of the way of support, as shown in Table 1.

A ring type vortex anemometer [8] was applied to measure the free stream velocity U within an uncertainty of ±3%. The laser displacement meter measured the displacement Z at one end of the cylinder outside the measuring section, as shown in Fig. 1, and its uncertainty was ±2%. The vortex shedding frequency f_v was obtained by applying FFT analysis to the streamwise fluctuating velocity u detected by a hot wire probe at a location in the near wake of the cylinder ($x=2b$, $z=1d$, see Fig. 1). Since the velocity signal u includes turbulence, the spectrum of u was averaged over 20 data and the vortex shedding frequency f_v was taken to be the frequency at the maximum peak of the averaged spectrum. Thus, the uncertainty in f_v is estimated to be around 2%.

Results and Discussion

The nondimensional vortex shedding frequency f^* and nondimensional root-mean-square (rms) value of displacement, Z_{rms}/d, are plotted against the reduced velocity V_r in Figs. 3–5 for the three cylinders supported by three different ways shown in Fig. 2. In one run of the wind tunnel experiment, V_r was first increased stepwise from the lowest value of around 2.5 to the highest value of around 20 by increasing the free stream velocity U, and then decreased again to the lowest nondimensional velocity. The corresponding Reynolds number Re is from 2000 to 16,000. In these figures, open symbols are for increasing V_r and solid symbols for decreasing V_r, respectively. When the twin plate spring was used, the oscillation behavior showed only a slight difference between

cases of ''in-phase'' and ''anti-phase'' settings, confirming that the cylinder motion is purely translational in these settings.

Cylinder I ($b/d=0.5$). Figure 3 shows f^* and $Z_{\rm rms}/d$ versus V_r of Cylinder I for (a) pure cross-flow oscillation ($\alpha_g=0$), (b) ''in-phase'' α_g, and (c) ''anti-phase'' α_g.

For the pure cross-flow oscillation shown in Fig. 3*a*, a sharp maximum peak in $Z_{\rm rms}/d$ appears at $V_r\approx 7$, showing the occurrence of Kármán vortex excitation. The frequency of this large amplitude oscillation is equal to the natural frequency f_n of translational motion. The nondimensional vortex shedding frequency f^* is equal to unity over a considerable range of nondimensional velocity around maximum oscillation, showing that the lock-in phenomenon is occurring there. The oscillation behaviors for the increasing V_r and the decreasing V_r agree well, which shows that the effect of hysteresis is insignificant in the pure cross-flow oscillation of Cylinder I. Galloping did not occur on Cylinder I when $\alpha_g=0$.

The lower oscillation peak at around $V_r=8$ is not due to the translational oscillation but caused by rotational oscillation around the x axis (see Fig. 1), since the phases of the displacement Z at both ends of the cylinder are anti-phase, as confirmed by measur-

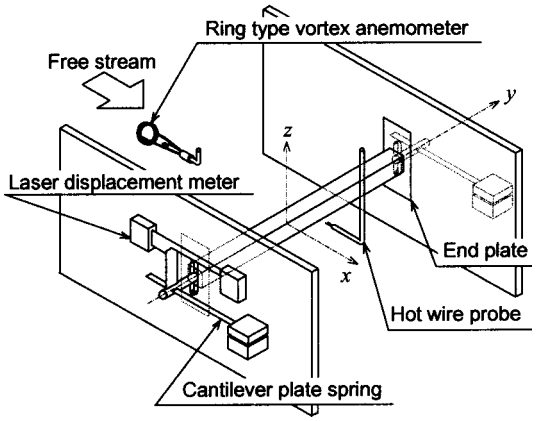

Fig. 1 Arrangement of the experimental apparatus and the coordinate system

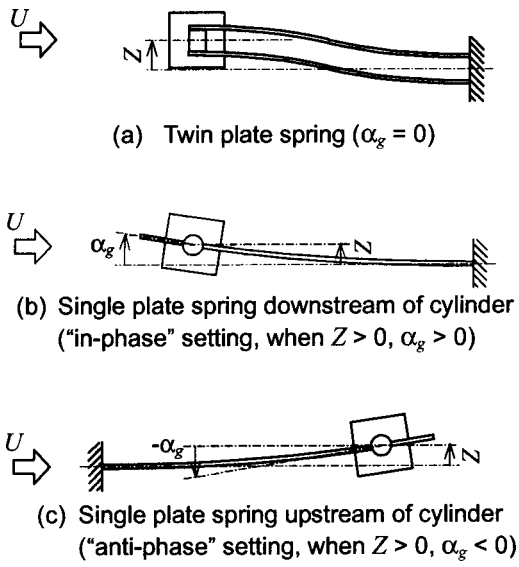

Fig. 2 Cylinder support method by cantilever plate spring and relationship between α_g and Z (flow direction is from left to right)

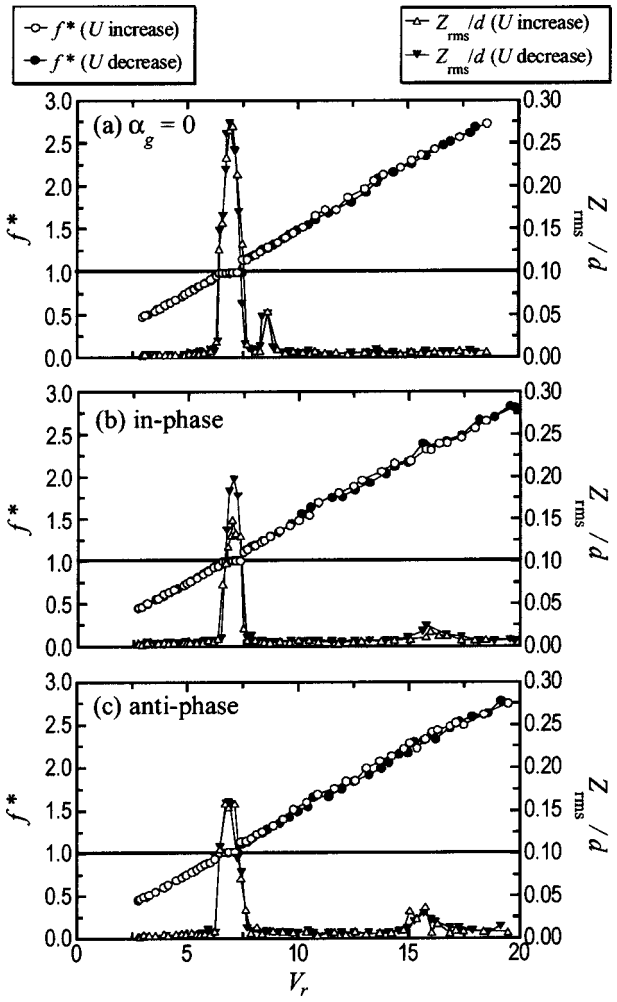

Fig. 3 f^* and $Z_{\rm rms}/d$ versus V_r for $b/d=0.5$

Table 1 Characteristics of the oscillating system

	Cylinder	b/d	k [N/m]	f_n [Hz]	m_e [kg]	δ
Single-plate spring	I	0.5	1260	17.0	0.11	0.011*1, 0.011*2
	II	1.0		16.7*1, 17.0*2		0.012*1, 0.011*2
	III	2.0		17.0		0.013*1, 0.012*2
Twin-plate spring	I	0.5	1310	17.0	0.12	0.013
	II	1.0		17.0		0.010
	III	2.0		17.0		0.012

*1''In-phase'' setting.
*2''Anti-phase'' setting.

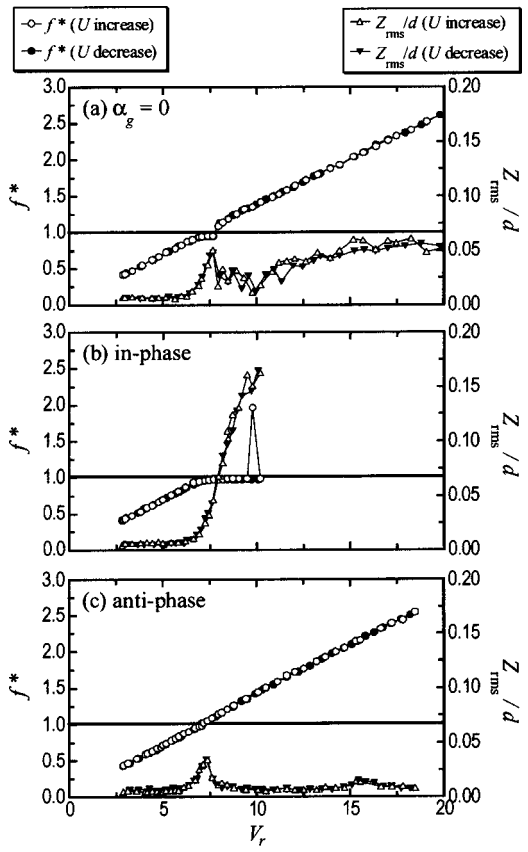

Fig. 4 ***f**** and Z_{rms}/d versus V_r for $b/d=1.0$

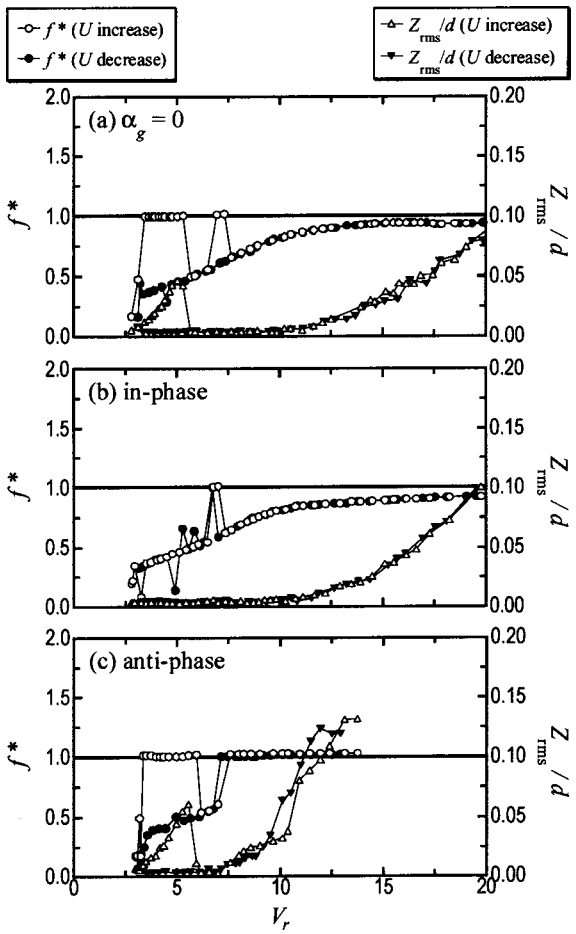

Fig. 5 ***f**** and Z_{rms}/d versus V_r for $b/d=2.0$

ing Z at both ends of the cylinder simultaneously. Furthermore, the oscillation frequency at this lower peak is confirmed to be equal to the natural frequency of the rotational mode oscillation around the x axis.

When "in-phase" or "anti-phase" α_g is superimposed, the oscillation behavior of Cylinder I is essentially equivalent to the pure cross-flow oscillation, as seen in Figs. 3*b* and 3*c*, except that the maximum Z_{rms}/d value becomes a little lower and the second peak in Z_{rms}/d at $V_r=8$ disappears while a much lower peak appears near $V_r=16$ instead. The latter effect is caused by the shift of the natural frequency of the rotational oscillation mode due to the support method.

Galloping does not occur on Cylinder I whether α_g exists or not. As a result, it is shown that the attack angle fluctuation α_g affects neither Kármán vortex excitation nor the galloping of Cylinder I, which has a slenderness smaller than the critical value.

Cylinder II ($b/d=1.0$). Figure 4 shows the oscillation behavior of Cylinder II. In the case of Cylinder II with $\alpha_g=0$, both Kármán vortex excitation and galloping are induced in different nondimensional velocity ranges, as seen in Fig. 4*a*. The large oscillation over the range of $V_r=7-8$ accompanied by lock-in phenomenon, i.e., the nondimensional vortex shedding frequency f^*, continues to be unity, showing the occurrence of Kármán vortex excitation. When the nondimensional velocity V_r is increased beyond this range, the oscillation amplitude decreases significantly and f^* returns to the value for the cylinder at rest, which shows that the Kármán vortex excitation ends at around $V_r=8$. When V_r is increased further, Z_{rms}/d begins to increase again while f^* is not equal to unity but proportional to V_r. The oscillation frequency is always equal to f_n while the cylinder oscillates. These behaviors of f^* show that cylinder oscillation shifts to galloping. Thus, in the case of Cylinder II with $\alpha_g=0$, both Kármán vortex excitation and galloping occur in their respective nondimensional velocity ranges.

Figures 4*b* and 4*c* show that the oscillation behaviors of Cylinder II with "in-phase" and "anti-phase" setting are dramatically different from the case of pure cross-flow oscillation ($\alpha_g=0$). As seen in Fig. 4*b*, the Z_{rms}/d of Cylinder II with "in-phase" setting traces that of Cylinder II with $\alpha_g=0$ until $V_r\approx 8$, where the Kármán vortex excitation is maximum in the case of $\alpha_g=0$. However, Z_{rms}/d continues to increase with V_r with an almost constant slope beyond $V_r\approx 8$ up to the maximum value of the experimental range at $V_r=10$. Throughout the region of large oscillation, the cylinder oscillates at its natural frequency f_n and the velocity spectrum S_u has a dominant peak at the frequency $f_v=f_n$, i.e., $f^*=1$, showing the occurrence of lock-in. However, S_u also had a peak at $2f_v$ in the large oscillation range as seen in the plot for f^* (dislocated plot, $f^*=2$) in Fig. 4*b*. Hence, the nondimensional velocity regions of Kármán vortex excitation and galloping can be no longer clearly distinguished by f^* and Z_{rms}/d in the case of in-phase α_g.

In the case of Cylinder II with "anti-phase" setting, in contrast, the Kármán vortex excitation is considerably suppressed and the lock-in region almost disappears, as seen in Fig. 4*c*. In addition, the galloping is almost completely suppressed.

The hysteresis in oscillation behavior of Cylinder II is also insignificant, as the case of Cylinders I, whether α_g is superimposed or not.

Thus, the influence of α_g on the oscillation behavior of Cylinder II is pronounced and its effects are in contrast depending on the phase difference between α_g and Z generated by the support

system. When α_g is in-phase with Z, both Kármán vortex excitation and galloping are strongly enhanced. In contrast, vortex excitation is significantly suppressed when α_g is anti-phase with Z, and galloping is almost entirely suppressed.

Cylinder III ($b/d=2.0$). Cylinder III with $\alpha_g=0$ shows the occurrence of two different oscillations with increasing V_r, i.e., low-velocity excitation in the range of $V_r=3-6$ and galloping in a higher nondimensional velocity range, say $V_r>12$, as seen in Fig. 5*a*. Kármán vortex excitation does not occur since the slenderness is larger than the Kármán vortex excitation region [9]. Since the range of V_r for the low-velocity excitation is much lower than the value of V_r at which $f^*=1$, i.e., $V_r=12$, its mechanism is not a synchronization between the cylinder oscillation and the periodic vortex shedding. Although f^* is equal to unity in this region and it seems to be lock-in, the peak in S_u at f_n is caused by velocity fluctuation due to the large cylinder oscillation. The galloping occurs when $V_r>12$ and the amplitude grows with V_r at an increasing gradient, showing the typical divergent character of galloping. When V_r is decreased, Z_{rms}/d traces the same curve in the galloping region but low-velocity excitation is not observed at all. This hysteretic behavior of the low-velocity excitation of Cylinder III is more pronounced compared with other excitations described in this paper, and it shows a strong nonlinearity of the low-velocity excitation.

In the case of Cylinder III with ''in-phase'' setting (Fig. 5*b*), the low-velocity excitation completely vanishes, while galloping is not affected by the superposition of α_g. In contrast, in the case of Cylinder III with ''anti-phase'' setting (Fig. 5*c*), the behavior of the low-velocity excitation including hysteresis is not affected by the superposition of α_g, while galloping occurs at a lower nondimensional velocity and its amplitude grows with V_r much more rapidly than in the case of $\alpha_g=0$. A sudden jump of f^* to unity appears at around $V_r=7$ in Figs. 5*a*–5*c*. This might be lock-in, but the cylinder oscillation is small at this V_r. Hence, the relation of the sudden jump of f^* to the oscillation is still to be investigated.

Conclusions

In this study, the cross-flow oscillation of a rectangular cylinder supported by a cantilever plate-spring system was investigated using a wind tunnel. Three kinds of supports were tested, which introduce different relationships between the geometrical attack angle α_g and cylinder displacement Z: (i) pure cross flow oscillation ($\alpha_g=0$), (ii) the phase difference ϕ between α_g and Z is zero (in-phase), and (iii) $\phi=\pi$ (anti-phase). Three rectangular cylinders with the slenderness of $b/d=0.5$, 1.0, and 2.0 were used to investigate the influence of α_g on Kármán vortex excitation and galloping.

The superposition of α_g has essentially no influence on the Kármán vortex excitation irrespective of b/d and ϕ, when the slenderness $b/d=0.5$ (Cylinder I). In the case of Cylinder II ($b/d=1.0$), the Kármán vortex excitation is considerably suppressed and the galloping is also completely suppressed when the cylinder is supported with ''anti-phase'' setting. In contrast, when the cylinder was supported with ''in-phase'' setting, the oscillation increases continuously beyond the nondimensional velocity V_r for the maximum amplitude of Kármán vortex excitation with $\alpha_g=0$, leading to galloping much larger than in the case of $\alpha_g=0$. In the case of Cylinder III ($b/d=2.0$), the influence of anti-phase α_g on the galloping of Cylinder III is opposite to that of Cylinder II, since the onset of galloping shifts to a considerably lower nondimensional velocity and its amplitude grows rapidly with V_r. However, the in-phase α_g does not affect the galloping on Cylinder III.

The above results show that the effect of attack angle fluctuation strongly depends on the slenderness b/d and ϕ, and it is stronger on galloping than on Kármán vortex excitation.

Acknowledgments

The support provided by the Hungarian Research Foundation (OTKA Project No. T 042961) is gratefully acknowledged by L. Baranyi.

Nomenclature

b = streamwise length of rectangular cross section
d = height of rectangular cross section
f_n = natural frequency
f_v = vortex shedding frequency
f^* = nondimensional vortex shedding frequency ($=f_v/f_n$)
k = spring constant
m_e = effective mass
Re = Reynolds number ($=Ud/\nu$, ν: kinematic viscosity)
U = free stream velocity
u = streamwise fluctuating velocity
V_r = Reduced velocity [$=U/(f_n d)$]
Z = displacement of rectangular cylinder
α_g = geometrical attack angle due to deflection of cantilever
δ = logarithmic damping factor

References

[1] Nakamura, Y., and Hirata, K., 1994, ''The Aerodynamic Mechanism of Galloping,'' Trans. J. Soc. Aero. Space Sci., **36**, No. 114, pp. 257–269.
[2] Bearman, P. W., and Obasaju, E. D., 1982, ''An Experimental Study of Pressure Fluctuations on Fixed and Oscillating Square-Section Cylinder,'' J. Fluid Mech., **119**, pp. 297–321.
[3] Chen, J. M., and Liu, C. H., 1999, ''Vortex Shedding and Surface Pressures on a Square Cylinder at Incidence to a Uniform Air Stream,'' Int. J. Heat Fluid Flow, **20**, pp. 592–597.
[4] Parkinson, G. V., and Brooks, N. P. H., 1961, ''On the Aeroelastic Instability of Bluff Cylinders,'' J. Appl. Mech., **28**, pp. 252–258.
[5] Deniz, S., and Staubli, T. H., 1997, ''Oscillating Rectangular and Octagonal Profiles: Interaction of Leading- and Trailing-Edge Vortex Formation,'' J. Fluids Struct., **11**, pp. 3–31.
[6] Khalak, A., and Williamson, C. H. K., 1999, ''Motions, Forces and Mode Transitions in Vortex-Induced Vibrations at Low Mass-Damping,'' J. Fluids Struct., **13**, pp. 813–853.
[7] Shirakashi, M., Ishida, Y., and Wakiya, S., 1985, ''Higher Velocity Resonance of Circular Cylinder in Cross Flow,'' Trans. ASME J. Fluids Eng., **107**, pp. 392–396.
[8] Koide, M., Takahashi, T., and Shirakashi, M., 2001, ''Development of a Ring-Type Vortex Anemometer for Low-Velocity Wind Tunnel Experiments,'' Bull. JSME, **67**, 657, B, pp. 1105–1111.
[9] Nakamura, Y., Hirata, K., and Urabe, T., 1991, ''Galloping of Rectangular Cylinders: Effects of a Downstream Splitter Plate,'' *Proc. of the 5th Int. Conf. on Flow Induced Vibration*, 20–22 May, Brighton, pp. 453–458.